ChemComm

COMMUNICATION

View Article Online
View Journal | View Issue

Cite this: *Chem. Commun.*, 2024, **60**, 14778

Received 23rd September 2024,
Accepted 11th November 2024

DOI: 10.1039/d4cc04915b

rsc.li/chemcomm

Living plant-assisted recycling of nano gold into Murray porous carbon electrode materials†

Jinling Li, Qianghong Wu, Huanzhong Zeng, Rong Zou, Jianzhou Niu, Junlong Chen, Hongjun Liu and Fen Ran *

Based on the enrichment potential of living plants for nanoparticles, this paper develops a new strategy to utilize Murray's law in plants to remove various shapes of gold nanoparticles and, *in situ*, convert them into Murray porous carbon. The inherent Murray network serves as an optimized hierarchical design and ensures the mechanical stability of the material, and Murray's law is employed to achieve uniform dispersion of nanoparticles *in vivo*, facilitating the preparation of metal nanoparticle-supported carbon materials.

Engineered nanoparticles (NPs) have become ubiquitous due to their applications in diverse domains. Among various NPs, Au NPs have demonstrated exceptional stability and witnessed a surge in catalysis, biomedicine, and energy storage. The market for Au NPs is expected to grow at a compound annual growth rate of 10.25% from 2023 to 2028.[1] As the production and use of Au NPs increase, their eventual release into the environment raises concerns about environmental safety and potential biological risks.[2] Studies have indicated that Au NPs enhance free radical scavenging as well as antioxidant enzymatic activities while influencing microRNA expression in plants.[3] Notably, Au NPs can enter the food chain through plants, thereby posing risks.[4] Consequently, there has been an increasing concern regarding the removal of Au NPs. At present, NPs removal technology includes improvements based on the coagulation and flocculation processes, membrane filtration, adsorption, and cloud point extraction. It is worth mentioning that these methods do not consider the reuse of recycled NPs. Considering that NPs are valuable, reusing these pollutants presents profit opportunities. Certain plant species, such as tomatoes, have been observed to have an inherent ability to uptake and accumulate Au NPs, implying that they may be effective in removing NPs.[5] In addition to plant species, previous studies have investigated how NPs size, shape, and surface properties influence their entry into plants.[6–8] Shapes are important in defining the behavior of NPs within plants because they influence modalities of internalization, translocation pathways, and ultimate cellular fate. Au NPs exhibit various shapes, such as spheres, rods, and stars, which can significantly impact their biological functions, comprising bio-distribution and cellular uptake efficiency. However, further investigation is required to focus on the enrichment of Au NPs of various shapes found in plant systems. In light of these factors, a model tomato is proposed to absorb Au NPs with varying geometries in a simulated water environment.

To further avoid secondary pollution caused by the plants' absorption of NPs, it is necessary to reuse them. As a natural biological adsorbent, plants, with their exquisite structure, abundant heteroatoms, and absorbed NPs, are highly suitable for the preparation of energy storage material. This presents a novel approach to the reuse of these valuable resources. Thus, the recovery of NPs by biological absorption is a low-cost, simple operation, and environmentally friendly approach. Scheme 1 shows the tomato uptake of Au NPs and their reuse as Murray porous carbon. The recycle and reuse process follows

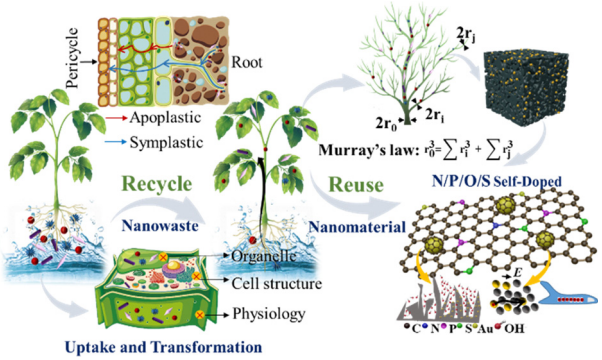

Scheme 1 Schematic for tomato uptake of different shapes of Au NPs and their reuse as Murray porous carbon materials.

State Key Laboratory of Advanced Processing and Recycling of Non-ferrous Metals, Department of Polymeric Materials Engineering, School of Material Science and Engineering, Lanzhou University of Technology, Lanzhou 730050, Gansu, China. E-mail: ranfen@lut.edu.cn, ranfen@163.com

† Electronic supplementary information (ESI) available. See DOI: https://doi.org/10.1039/d4cc04915b

three steps: uptake of Au NPs in living tomatoes, pre-oxidation, and carbonization to form Murray porous carbon.

In order to assess how the shape influences the absorption processes of Au NPs, four varieties of Au NPs are prepared: spherical Au NPs, nanorod Au NRs, nanobipyramid Au NBPs, and nanostar Au NSs. A particle count conducted using various TEM images of the sample verified the existence of monodispersed Au NPs, along with their average diameter or width (Fig. S1a–h, ESI†). The results of UV-Vis spectroscopy are illustrated in Fig. S1i–l (ESI†).

Tomatoes are initially cultivated in solutions of various shapes of Au NPs at a concentration of 100 mg L^{-1}. In order to assess the effects on tomato growth, the growth process is systematically recorded (Fig. S2a, ESI†). When seedlings are subjected to a 40 h exposure, all plants exhibit varying degrees of impact in comparison to the control. Among them, in Au NRs, tomato stems show obvious wilting (Fig. 1a), and roots are seriously atrophied. This is attributed to the Au NRs blocking of cell walls or plasma membrane pores, thus hindering the transport and transfer of water and nutrients (Fig. 1b). This research aligns with the toxicity mechanisms of NPs as outlined by X. Bai *et al.*[8] Fig. S3 (ESI†) displays the cross-sections of the stem containing Au NRs, taken with a laser confocal microscope, confirming that there is a significant coating present on the stem.

In Au NSs, the roots and stems of the tomatoes are intact. However, most of the leaves are dry (Fig. 1c). This is attributed to the presence of more ''hot spots'' of local plasma electric field in Au NSs (Fig. 1d). In 2024, Luo *et al.* and Shao *et al.* reaffirmed the significant electric field effect at the apex of the Au NSs through finite-difference time-domain (FDTD) simulations and finite element method (FEM) analyses.[9,10] Therefore, the morphology of Au NPs plays a noteworthy role in plant response. UV-Vis revealed strong absorption peaks in 320–400 nm. This suggests that the presence of Au NSs and Au NBPs enhance the plants' ability to absorb ultraviolet rays (Fig. S4, ESI†). This is consistent with the dry leaf effect noted in the Au NSs group.

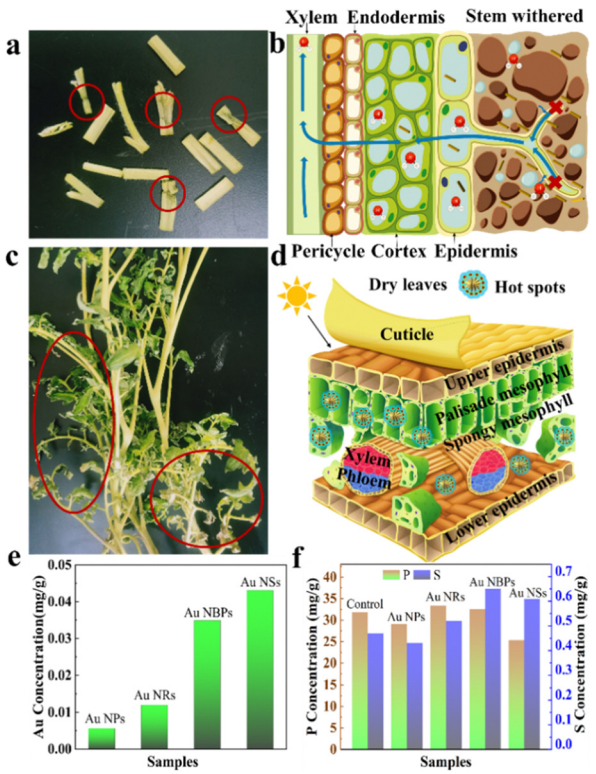

Fig. 1 (a) The wilting of tomato stems after being exposed to Au NRs for 40 h, along with the underlying causes (b). (c) Leaf drying induced by Au NSs, along with the causes of shot spots (d). (e) and (f) The levels of Au, P, and S in tomatoes.

In order to assess the capacity of tomatoes to uptake Au NPs, the Au concentration is quantified using ICP-OES. The Au NSs are the highest, followed by Au NBPs. At the same time, the Au NRs and Au NPs are relatively less (Fig. 1e). Consequently, it can be inferred that tomatoes cells absorb non-spherical NPs more rapidly and in greater amounts than its do spherical NPs. The morphology of Au NPs affects the symmetry of curvature energy, which in turn impacts the endocytic routes and the angle of internalization during endocytosis. Our findings align with the interaction mechanism between NPs of varying shapes and cell membranes, as simulated by Wei *et al.* in 2021.[11]

To examine the impact of Au NPs on P and S, an analysis of the elemental composition within the plant is conducted following the absorption of contaminated liquid. ICP data show that compared with the control, Au NRs and Au NBPs promote P absorption, while Au NPs and Au NSs inhibit P absorption. Except for Au NPs, other shapes of Au NPs all promoted the absorption of S (Fig. 1f). It is believed that the presence of Au NPs influences S uptake in tomatoes and enhances the expression of genes and transport proteins related to S assimilation.[12] EDS images of P, S, and Au also confirmed this phenomenon (Fig. S5, ESI†). Various shapes of Au NPs exhibit different plant toxicity and can also affect the absorption of nutrient elements.

TG and DTG analyses were performed to investigate the Au content and its impact on the pyrolysis kinetics of contaminated biomass. The mass ratio of samples after heating to 800 °C follows the order of Au NPs < control < Au NRs < Au NBPs < Au NSs (Fig. S6a, ESI†), which is consistent with the ICP test results.

All the above confirms that the shape of Au NPs affects the amount of exocytosis. In tomatoes, there are two main ways to absorb and transport Au NPs. The first is the apoplastic pathway, and the second way is the symplastic pathway.[13]

In order to avoid secondary pollution and improve the value of biomass, the plants adsorbed Au NPs are dried and carbonized at 800 °C for 3 h. The DTG (Fig. S6, ESI†) illustrates that Au NSs have two distinct effects on the pyrolysis of biomass. And SEM (Fig. S7, ESI†) shows that bio-char is a laminated structure with long parallel channels that are related to the extensive vascular and elongated tissue cells of a plant. High-resolution SEM of 3DC-Au NSs (Fig. 2a) shows transverse holes from the plant's pits. During calcination, Murray porosity is preserved. Plants have evolved fractal-like vascular systems that follow Murray's law to maximize hydraulic conductance while minimizing the transport barrier to water and nutrients. Water traverses the cell cavity with ease, ascending along the stem. The pores in the side walls allow water to flow laterally into the surrounding parenchyma cells. Fig. S8 (ESI†) presents the hierarchical models abstracted from plant Murray systems. It

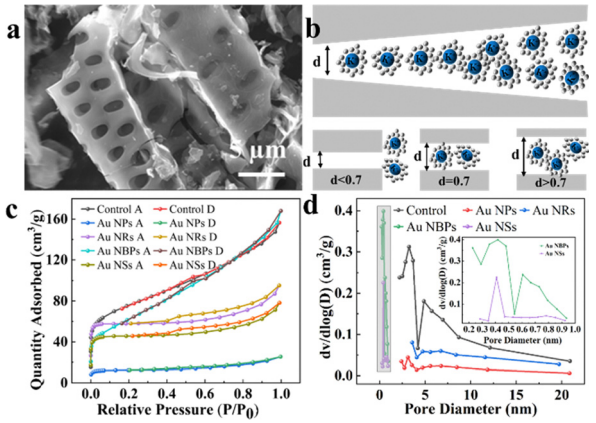

Fig. 2 (a) SEM confirmed the reservation of Murray pores in 3DC-Au NSs. (b) Schematic diagram of hydrated potassium ion energy storage. (c) Nitrogen adsorption–desorption isotherms and pore size distribution (d) of all samples.

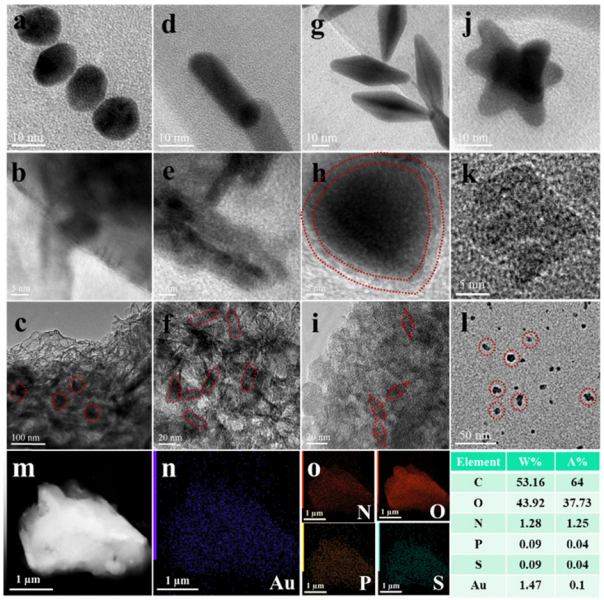

Fig. 3 (a) TEM image of Au NPs and 3DC-Au NPs with different resolutions (b) and (c). (d)–(f) Au NRs. (g)–(i) Au NBPs. (j)–(l) Au NSs. (m) HAADF-STEM of 3DC-Au NSs and its mapping (n) and (o).

comprises a parent pore with a radius denoted as r_0, which is linked to multiple child pores by r_i and r_j, facilitating the transfer and exchange of substances. A three-dimensional network is optimal for achieving high efficiency in mass transportation. The larger channels play a crucial role in the swift movement of electrolytes, whereas the smaller channels and pores are essential for the effective delivery of ions and nutrients.

In Fig. 2c, 3DC-Au NRs, 3DC-Au NRs, and 3DC-Au NBPs exhibit a standard H4 hysteresis. In comparison with the control, the specific surface area increased in all groups except for the 3DC-Au NSs (Table S1, ESI†). During the carbonization process, the production of small molecular gases facilitates the formation of pores. Also, small Au NPs are embedded in the carbon, increasing the specific surface area. The reduction in 3DC-Au NSs can be explained by the increased absorption of Au NSs and the obstruction of certain holes, aligning with findings from studies on different metal loadings.[14] The larger adsorption capacity, the greater number of micro-pores, which is beneficial for the formation of EDLC.[15] Such hierarchical Murray pores are conducive to constructing a continuous network, given that a channel for electrolyte ions to enter the carbon layer and facilitate the diffusion and transfer. In Fig. 2d, the pore size distribution of 3DC-Au NSs exhibited a relatively dense micro-pore at 0.4 and 0.7 nm. When the pore size is less than 1 nm, the capacitance of the material will increase abnormally.[16] The existence of intermediate pores facilitates charge transfer pathways, whereas micro-pores contribute to the maintenance of the specific surface area.[17] Fig. 2b shows the schematic of energy storage under a wedge slit. Pores smaller than 0.7 nm do not have enough space for K^+ to complete insertion and removal.

TEM images of Au NPs and 3DC-Au NPs are shown in Fig. 3. According to the HRTEM images in Fig. 3(b), (e), (h) and (k), various shapes of Au NPs are embedded in Murray porous carbon, with a lattice spacing of 0.235 nm, conforming to Au (111). Au NSs have obvious apexes; however, when prepared to carbon material, some apexes are retained, but some are no longer sharp. This phenomenon may be attributed to the alteration of Au NPs by enzymes where their absorption by plants. But all Au NPs are tightly sealed in the matrix, and Fig. 3(c)–(l) clearly shows the porous structure. Au NPs with diverse geometries, when combined with a carbon matrix, create unique metal-support interfaces. These interfaces can lead to a rearrangement of the Fermi level, reducing the reaction energy barrier. Au NSs have more vertices and form more metal-support interfaces with the carbon matrix. Fig. 3m presents a representative HAADF-STEM image of 3DC-Au NSs. Fig. 3n–o displays the distribution of Au, N, O, P, and S, showing that these elements are evenly spread out. These findings indicate that the even distribution of Au in 3DC-Au NSs is achieved using a plant absorption method. As illustrated in Fig. 3 the atomic ratios of C, Au, N, O, P, and S were 64 : 0.1 : 1.25 : 37.73 : 0.04 : 0.04. The SEM-EDS mapping (Fig. S9, ESI†) also showed that the distribution of elements is uniform.

Fig. S10 (ESI†) show the high-resolution XPS spectra of C, N, P, S, and Au in 3DC-Au NSs and the control. Table S2 (ESI†) displays the proportion of various N, P, and S types before and after Au NSs enrichment. The presence of Au significantly elevates the fraction of N–Q, which is attributed to Au's catalytic role in the graphitization of carbon. And Au can be divided into two peaks: 84.0 eV for Au $4f_{7/2}$, and 89.0 eV for Au $4f_{5/2}$ (Fig. S10f, ESI†). This indicates that Au NSs still exist at zero valence after being absorbed by tomatoes.

Compared to the control, the FTIR peak of the pyrolysis products on 3DC-Au NSs shows a shift and an increase in intensity (Fig. S10g, ESI†). The N–H (3, 500^{-3}, 300 cm^{-1}) stretching vibration indicates that 3DC-Au NSs have more N, supporting XPS results. The peaks at 1, 270 cm^{-1} and 680 cm^{-1} correspond to C–S and C–P. The I_D/I_G of 3DC-Au NPs materials with various shapes is 0.85 (Fig. S10h, ESI†). It suggests that the graphitization with different shapes Au NPs is higher. The XRD patterns of the five carbon samples exhibit identical characteristics (Fig. S11, ESI†).

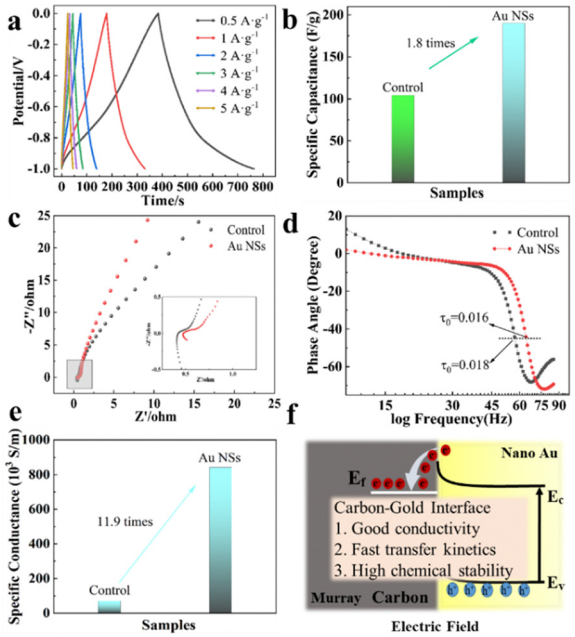

Fig. 4 (a) GCD curves of 3DC-Au NSs. (b) Histogram of the surface capacity of control and 3DC-Au NSs. (c) EIS responses, Bode plots (d), and four-electron probe test (e) of control and 3DC-Au NSs. (f) Outstanding advantages of nano Au at 3DC-Au NSs.

The specific capacitance of 3DC-control, 3DC-Au NPs, 3DC-Au NBPs, 3DC-Au NRs, and 3DC-Au NSs are 104.4, 154.4, 162.3, 178.4, and 190.2 F g^{-1}, respectively (Fig. S12, ESI†). Fig. 4a show the GCD curves of 3DC-Au NSs. Its specific capacitance is 1.8 times higher than the control (Fig. 4b). This is due to the tomatoes absorbing more Au NSs, and Au NSs have more edges and corners, so more metal-support interfaces with carbon materials are formed. The CV and GCD curves of other samples are presented in Fig. S12 and S13 (ESI†). Fig. 4c and d shows the contrast diagrams of impedance and phase angle of the control and 3DC-Au NSs. The slope of 3DC-Au NSs in the low-frequency region is greater than the control. This indicates that the 3DC-Au NSs have better ion diffusion and near-ideal capacitance. The time constant τ_0 ($\tau_0 = 1/f_0$) of 3DC-Au NSs is only 16 ms. While the τ_0 of the control is 18 ms, the shorter τ_0 implies a fast ion transport rate. The four-probe technique was employed to further assess the conductivity of the samples, demonstrating that the Au NSs significantly improved conductivity, as illustrated in Fig. 4e. Fig. S14 (ESI†) provides an overview of the proportions of capacitive and pseudo-capacitive contributions in 3DC-Au NSs. At 5 mV s^{-1}; the contribution of EDLC is 45.1%, while the pseudo-capacitance is 54.9%. When the scan rate is increased to 100 mV s^{-1}, the EDLC reaches 79.2%. This is mainly due to the excellent electronic conductivity, and fast ion diffusion of 3DC-Au NSs (Fig. 4f). The stability test is presented in Fig. S15 (ESI†).

The research indicates that extracting Au NPs from tomatoes and creating electrode materials is both practical and cost-effective. To make bioremediation for new pollutants more effective, it is important to deal with the problems that come up when organisms don't absorb these substances well and the process takes a long time. This issue will remain a subject of an ongoing investigation in future research endeavors.

In conclusion, this research develops a new strategy that utilizes Murray's law in plants to remove various shapes of Au NPs and convert them into electrode materials. The electrode material features a 3D hierarchically porous framework that adheres to Murray's law, enhancing electrolyte diffusion, facilitating electron/ion transfer, and offering robust chemisorption for electrolytes. Even more interesting is that NPs absorbed by plants are well-distributed in the triple carbon derived from the cell wall, cytomembrane, and tonoplast. This approach can be further developed to facilitate the recycling of additional nanomaterials by employing a variety of plant species to generate a wide array of composites with tailored chemical composition, physical structures, and specific electronics.

J. L. Li: writing – review & editing, formal analysis, methodology and conceptualization. Q. H. Wu: methodology. H. Z. Zeng: software, investigation. R. Zou: validation. J. Z. Niu and J. L. Chen: visualization. F. Ran: funding acquisition, reviewing & editing. H. J. Liu: supervision.

This work was supported by the National Natural Science Foundation of China (52073133) and the Key Talent Project Foundation of Gansu Province.

Data availability

The data supporting this article have been included as part of the ESI.†

Conflicts of interest

There are no conflicts to declare.

Notes and references

1 S. S. Y. Law, T. Miyamoto and K. J. Numata, *Chem. Commun.*, 2023, **59**(47), 7166–7181.
2 Grand View Research, Inc, 2022, 978-1-68038-312-6.
3 K. S. Siddiqi and A. Husen, *Nanoscale Res. Lett.*, 2016, **11**, 400.
4 J. L. Ferry, P. Craig, C. Hexel, P. Sisco, R. Frey, P. L. Pennington, M. H. Fulton, I. Scott, A. W. Decho, S. Kashiwada, C. J. Murphy and T. J. Shaw, *Nat. Nanotechnol.*, 2009, **4**(7), 441–444.
5 H. Li, X. Ye, X. Guo, Z. Geng and G. Wang, *J. Hazard. Mater.*, 2016, **314**, 188–196.
6 Y. Y. Zhou, X. Liu, X. Yang, G. D. Laing, Y. Yang, F. M. G. Tack and M. S. Bank, *Environ. Sci. Technol.*, 2023, **57**(9), 3733–3745.
7 H. Zhang, N. S. Goh, J. W. Wang, R. L. Pinals, E. González-Grandío, G. S. Demirer, S. Butrus, S. C. Fakra, A. Flores, R. Zhai, B. Zhao and S. Park, *Nat. Nanotechnol.*, 2021, **17**(2), 197–205.
8 Y. C. Zhao, A. Du, T. Ge, G. Li, X. Q. Lian, S. F. Zhang, C. Hu and X. F. Wang, *J. Hazard. Mater.*, 2024, 135892.
9 M. N. Kang, Y. Z. Weng, Y. Liu, H. K. Wang, L. Ye, Y. L. Gu and X. Bai, *Rev. Environ. Contam. Toxicol.*, 2023, **261**(1), 5.
10 T. T. Zhao, X. Z. Pang, C. K. Wang, L. Wang, Y. F. Yang, J. Q. Wang, J. F. Jia and X. X. Liu, *Anal. Chem.*, 2024, **96**(11), 4402–4409.
11 X. Zhang, G. Ma and W. Wei, *NPG Asia Mater.*, 2021, **13**(1), 52.
12 N. Ohkama, K. Takei, H. Sakakibara, H. Hayashi, T. Yoneyama and T. Fujiwara, *Plant Cell Physiol.*, 2002, **43**(12), 1493–1501.
13 J. Lv and P. Christie, *Environ. Sci.: Nano*, 2019, **6**(1), 41–59.
14 H. Ma, Z. Chen, X. Gao and W. Liu, *Sci. Rep.*, 2019, **9**(1), 17065.
15 J. Wu, *Chem. Rev.*, 2022, **122**(12), 10821–10859.
16 J. Chmiola, G. Yushin, Y. Gogotsi, C. Portet, P. Simon and P. Taberna, *Science*, 2006, **313**(5794), 1760–1763.
17 T. Liu, F. Zhang, Y. Song and Y. Li, *J. Mater. Chem. A*, 2017, **5**(34), 17705–17733.